IntraVital 3, e29748; July 2014; © 2014 Landes Bioscience

Quantitative intravital two-photon excitation microscopy reveals absence of pulmonary vaso-occlusion in unchallenged Sickle Cell Disease mice

Margaret F Bennewitz[1,2], Simon C Watkins[3], and Prithu Sundd[1,2,*]

[1]Heart, Lung, Blood and Vascular Medicine Institute; University of Pittsburgh; Pittsburgh, PA USA; [2]Division of Pulmonary, Allergy and Critical Care Medicine; University of Pittsburgh; Pittsburgh, PA USA; [3]Center for Biologic Imaging; University of Pittsburgh; Pittsburgh, PA USA

Keywords: two-photon microscopy, sickle cell disease, red blood cells, vaso-occlusion, acute chest syndrome, neutrophils.

Sickle cell disease (SCD) is a genetic disorder that leads to red blood cell (RBC) sickling, hemolysis and the upregulation of adhesion molecules on sickle RBCs. Chronic hemolysis in SCD results in a hyper-inflammatory state characterized by activation of circulating leukocytes, platelets and endothelial cells even in the absence of a crisis. A crisis in SCD is often triggered by an inflammatory stimulus and can lead to the acute chest syndrome (ACS), which is a type of lung injury and a leading cause of mortality among SCD patients. Although it is believed that pulmonary vaso-occlusion could be the phenomenon contributing to the development of ACS, the role of vaso-occlusion in ACS remains elusive. Intravital imaging of the cremaster microcirculation in SCD mice has been instrumental in establishing the role of neutrophil-RBC-endothelium interactions in systemic vaso-occlusion; however, such studies, although warranted, have never been done in the pulmonary microcirculation of SCD mice. Here, we show that two-photon excitation fluorescence microscopy can be used to perform quantitative analysis of neutrophil and RBC trafficking in the pulmonary microcirculation of SCD mice. We provide the experimental approach that enables microscopic observations under physiological conditions and use it to show that RBC and neutrophil trafficking is comparable in SCD and control mice in the absence of an inflammatory stimulus. The intravital imaging scheme proposed in this study can be useful in elucidating the cellular and molecular mechanism of pulmonary vaso-occlusion in SCD mice following an inflammatory stimulus.

Introduction

Sickle cell disease (SCD) is an autosomal recessive genetic disorder affecting ~100,000 Americans and millions of people worldwide.[1] Sickle cell anemia (SCA) is the most common form of SCD and is caused by a homozygous mutation that results in the substitution of valine (Val) for glutamate (Glu) at the sixth position in the β-globin chain of hemoglobin.[2] The mutated hemoglobin, hemoglobin S (HbS), expressed inside red blood cells (RBCs) causes several chronic cellular complications including RBC sickling, RBC hemolysis and an enhanced expression of adhesion molecules on the RBC membrane.[3] The process of RBC hemolysis leads to a hyper-inflammatory state in SCD characterized by the chronic activation of circulating leukocytes, platelets and the vascular endothelium, as well as upregulation of inflammatory cytokines.[4-6]

Crisis in SCD patients can be precipitated by an inflammatory stimulus like a bacterial infection or sepsis, which leads to amplification of the hyper-inflammatory state, enabling leukocytes, platelets, pro-adhesive sickle RBCs (sRBCs) and endothelial cells to interact with each other to cause vaso-occlusion.[7,8] Vaso-occlusion can occur within the liver, spleen, lung, brain and bone marrow, and leads to ischemia-reperfusion injury-induced organ damage,[9] extracellular hemin crisis[7,10] and severe episodes of pain.[11] Vaso-occlusive pain crisis is the primary cause of emergency medical care for SCD patients and episodes of vaso-occlusive pain can occur several times a year and usually last for five to seven days.[2,12-14]

Vaso-occlusion has been studied primarily in the systemic microcirculation of the cremaster muscle,[15,16] mesentery,[17] skin[7] and the skull bone marrow[18] of transgenic mouse models of SCD using trans-illumination or epifluorescence intravital microscopy. Intravital imaging studies of the cremaster microcirculation in SCD mice have revealed that sRBCs and platelets interact with adhered neutrophils to orchestrate vaso-occlusion in the systemic postcapillary venules following addition of an inflammatory stimulant like tumor necrosis factor (TNF)-α.[15,19,20] Turhan et al.[19] found that while there was no binding between adherent leukocytes (primarily neutrophils) and RBCs in the cremaster venules of normal mice, neutrophil-sRBC interactions began 30 min after cremaster muscle surgery in SCD mice and further increased after TNF-α administration to cause vaso-occlusions. The neutrophil-sRBC interactions were mediated by the CD11b/CD18 (Mac-1) integrin on neutrophils binding to an unknown

*Correspondence to: Prithu Sundd; Email: prs51@pitt.edu
Submitted: 04/25/2014; Revised: 06/17/2014; Accepted: 06/26/2014; Published Online: 07/07/2014
http://dx.doi.org/10.4161/intv.29748

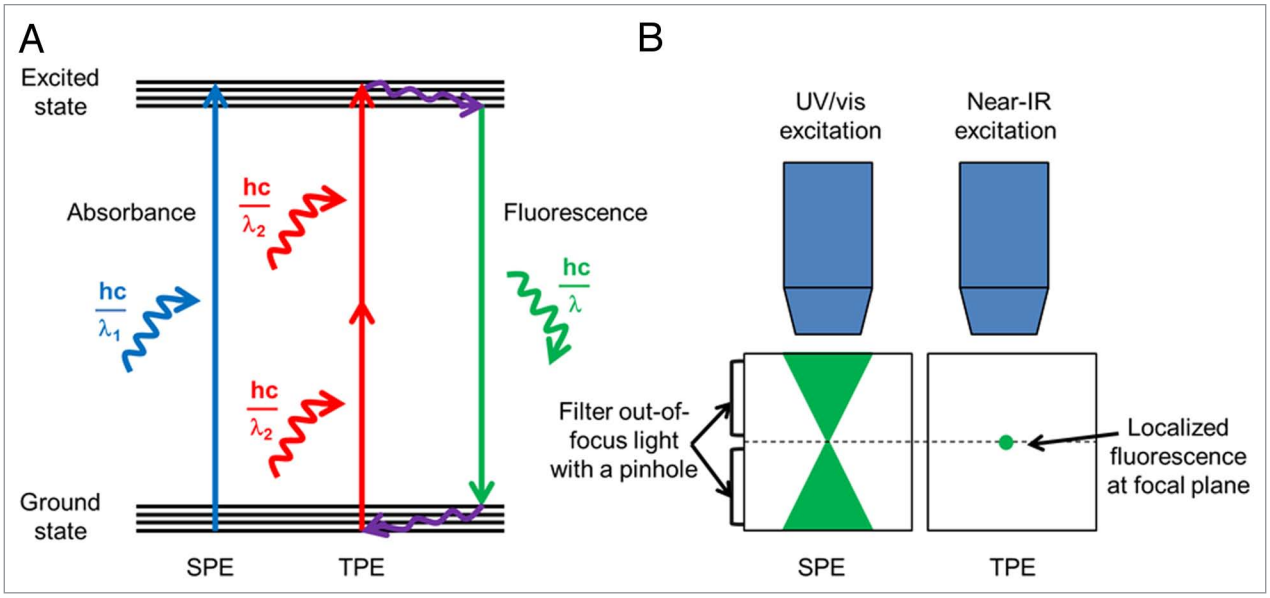

Figure 1. Comparison of single photon excitation (SPE) with two-photon excitation (TPE). (**A**) A single photon of higher energy ($E = hc/\lambda_1$) is absorbed in SPE to produce fluorescence emission. In TPE, two lower energy photons (each with $E = hc/\lambda_2$) are absorbed nearly simultaneously to produce the same fluorescence effect. Near-infrared lasers are used in TPE, which emit photons that have double the wavelength of photons used in SPE ($\lambda_2 = 2\lambda_1$). hc/λ is the energy of a photon, h is Planck's constant, c is the speed of light, and λ is wavelength. (**B**) In SPE techniques, such as confocal microscopy, a cone of fluorescent light is emitted within the sample. To obtain an image localized to the focal plane, a pinhole must be used to filter the out-of-focus light in SPE. In TPE, fluorescence is inherently localized to the focal plane and thus all emitted photons can be collected. The localized fluorescence in TPE leads to less phototoxicity and less photobleaching as compared with SPE.

ligand on sRBCs.[15] By knocking out the genes encoding the adhesion molecules involved in leukocyte rolling along inflamed venules (P-selectin and E-selectin), leukocyte rolling and adhesion was greatly reduced. Subsequently, leukocyte-sRBC interactions and the occurrence of vaso-occlusion were also decreased, leading to a reduction in mortality of SCD mice. Although these studies of the cremaster muscle have provided invaluable insight into the cellular and molecular mechanism of vaso-occlusion within the systemic microcirculation, the cremaster muscle is not known to be the primary site of vaso-occlusive pain crisis in SCD patients.[2,21]

SCD patients suffering from acute pain episodes often develop acute chest syndrome (ACS) within 2–3 d following hospitalization.[13,14] ACS is a form of acute lung injury and is characterized by fever, cough, chest pain, a new pulmonary infiltrate on a chest X-ray, enhanced hemolysis and high blood leukocyte counts. Most importantly, ACS is among the leading cause of mortality and morbidity among SCD patients.[13,14] Based on the clinical finding that ACS can occur following severe vaso-occlusive pain crisis, it is hypothesized that pulmonary vaso-occlusion could be the potential trigger driving the ACS.[8,13,14] Understanding the role of pulmonary vaso-occlusion in ACS and elucidating the cellular and molecular mechanism that may drive it can contribute to the development of new prophylactic and post crisis therapies to prevent ACS and patient mortality. However, this requires molecular studies of the lung microcirculation in SCD mice using real-time intravital microscopy. To date, such studies have never been performed.

Intravital imaging of the intact lung of live mice offers numerous technical challenges. In a live mouse, the lung vasculature experiences large scale movements (on the order of millimeters) from expiration/inspiration, the cardiac cycle, and pulsatile blood flow.[22-24] In addition to the dynamic movement of the lung, the tissue itself is very fragile and can be easily injured through accidental contact with surgical instruments, necessitating extra care during surgical preparation. Furthermore, visualizing cellular trafficking in real-time within the pulmonary microcirculation necessitates the use of fluorescence imaging techniques, such as two-photon excitation (TPE) microscopy or confocal microscopy, due to their high resolution in the z-direction compared with epifluorescence microscopy.[25] However, reaching high penetration depths with fluorescence imaging has been challenging due to the scattering of light within the lung tissue at the air-liquid interfaces.[22] For live tissue imaging, TPE microscopy is superior to confocal microscopy.[25] TPE microscopy involves the simultaneous absorption of two near-infrared (NIR) photons to excite a fluorochrome instead of the single photon absorption employed by confocal microscopy (**Fig. 1**). In contrast to confocal microscopy, which utilizes a pinhole to exclude out-of-focus light and generate z-stacks, TPE inherently allows optical sectioning of tissue in the z-direction. In TPE, the probability of simultaneous absorption of two photons is greatly confined to the focal plane of excitation, and thus produces localized fluorescence only at the focal plane.[25] In addition, TPE has other advantages over confocal techniques, as it exhibits reduced photobleaching, less phototoxicity, and an improved signal-to-noise ratio. Furthermore,

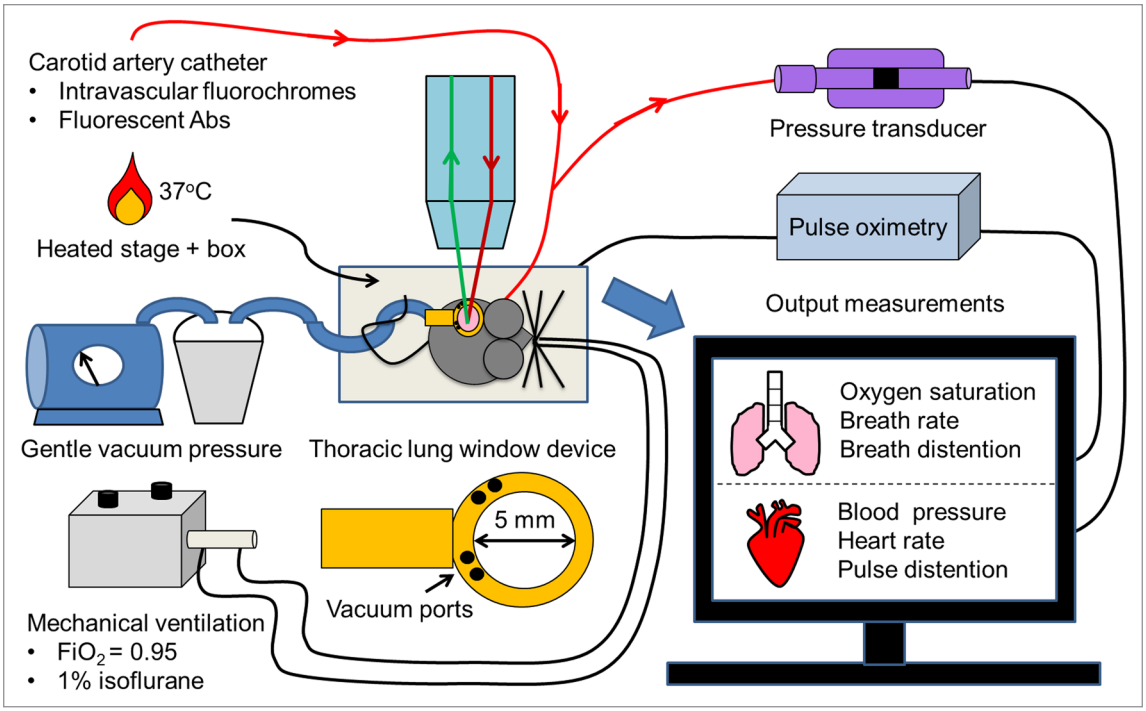

Figure 2. Schematic of our TPE imaging setup. A catheter is placed into the carotid artery to enable iv delivery of intravascular fluorochromes and fluorescent antibodies. The mouse is intubated to facilitate mechanical ventilation and delivery of 1% isoflurane with FiO_2 of 0.95. The temperature of the mouse is maintained with a heated stage and a temperature controlled enclosure surrounding the TPE microscope stage. Gentle vacuum suction is applied to the thoracic window device to immobilize a small region of the left lobe of the lung against a cover glass. TPE imaging is performed with a NIR laser. In the objective, red denotes excitation and green denotes emission fluorescence. The carotid artery catheter is also connected to a pressure transducer to monitor blood pressure during imaging. Pulse oximetery is used to monitor blood oxygen saturation, breath rate, breath distension, heart rate, and pulse distention.

TPE utilizes NIR wavelengths (> 700 nm) generated by a short-pulsed laser emitting excitation pulses of 10^{-13} s duration and 10^{-8} s apart, which leads to deeper tissue penetration (50–100 μm for lung tissue) than confocal microscopy.[25]

Recently, Looney et al.[23] introduced a novel method to stabilize a small area of the mouse lung through the application of a gentle vacuum (suction). The gentle immobilization served to minimize x-y lung movement from millimeters to within 5–10 microns. This approach enabled real-time visualization of leukocyte trafficking within the pulmonary microcirculation of wild type (WT) C57BL/6 mice and transgenic mice expressing fluorescent cells. In this study, we have used a modification of the methodology proposed by Looney et al.[23] to visualize real-time trafficking of blood cells in the pulmonary microcirculation of mechanically ventilated live SCD mice using TPE microscopy. In this study, we demonstrate the surgical, ventilation, fluorescence imaging and image analysis strategies that will enable other researchers to perform intravital studies to investigate pulmonary vaso-occlusion in SCD mice. We show that our experimental approach allows stable visualization of RBC and neutrophil trafficking within the lung microcirculation of live SCD mice under physiological conditions, and that the cellular trafficking within SCD mice is comparable to control mice in the absence of any inflammatory stimulus.

Results

Vacuum enabled thoracic window allows stable visualization of the pulmonary microcirculation and alveoli in live wild type mice

To enable TPE imaging of the lung microcirculation in live mice, we have utilized a modified thoracic window device (**Fig. 2**). The device applies a gentle vacuum (negative pressure) to immobilize the pleural surface of the left lobe of the mouse lung against a glass coverslip. We used WT C57BL/6 mice to establish the protocol for intravital lung imaging. Upon intra-arterial administration of FITC-dextran, our approach enabled visualization of the pulmonary microcirculation and alveolar air spaces (**Fig. 3**). **Figure 3** shows that the pulmonary capillaries surrounding the alveoli move dynamically in the z-direction as a result of the expansion and contraction of the air spaces from mechanical ventilation. However, the movement of the pulmonary capillaries in the x-y plane within the field of view is minimal. Real-time videos of the microcirculation show robust perfusion, as the fluorescent dextran flows through the vasculature and around RBCs, which appear as dark spots in the capillaries and feeding arteriole (**Movie S1**). The dynamic movement of alveoli and robust perfusion confirm that the thoracic window does not impede breathing and blood flow.

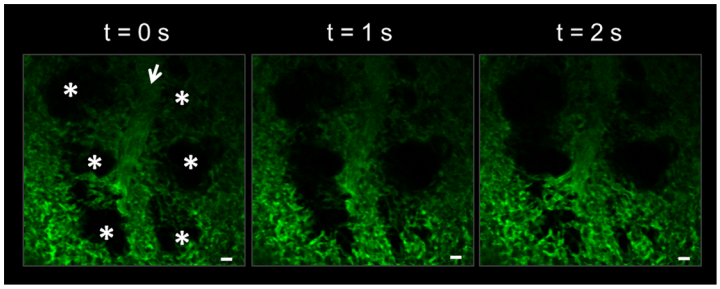

Figure 3. Vacuum enabled thoracic window allows for stable visualization of the pulmonary microcirculation and alveoli in a live C57BL/6 mouse. The pulmonary capillaries surrounding the alveoli (*) can be seen moving in and out of the imaging plane in the z-direction due to the dynamic expansion and contraction of the alveoli (*) with mechanical ventilation. Movement of alveoli starts from the bottom of the image at t = 0 s and moves up to the top with increasing time. Alveoli are marked by asterisks. Intravascular FITC dextran highlights the pulmonary capillaries and a feeding arteriole in green. The open arrow denotes the direction of blood flow within the feeding arteriole. The times displayed are relative to the selected video frames. Scale bars are 20 μm. The feeding arteriole has a diameter of 33 μm, while the capillaries have an average diameter of 6 ± 2 μm. The complete video sequence is included in **Movie S1**.

Elongated neutrophils slowly transit or rapidly 'hop' through the pulmonary capillaries in live WT mice

We next visualized neutrophil trafficking within the pulmonary microcirculation in live C57BL/6 WT mice using fluorescent monoclonal antibodies (mAbs) against Ly-6G or Gr-1, differentiation markers specific to neutrophils.[16,26] As shown in **Figure 4**, neutrophils are present in large numbers in the non-inflamed lung and elongate as they travel through pulmonary capillaries. Real-time videos (**Movie S2**) demonstrate that neutrophil trafficking is a combination of 'hopping (stop and go)' neutrophils and slowly transiting neutrophils. In both cases, the neutrophils completely fill the lumen of pulmonary capillaries, which are mostly smaller in diameter than the neutrophils.[27,28] Here, we have shown that some capillaries even in the non-inflamed lung are effectively occluded temporarily as neutrophils transit slowly through them, which can take longer than 5 min as shown previously.[29] These observations are supported by previous studies,[27,30-32] which have shown evidence of a large marginated pool of neutrophils within the pulmonary capillaries. The marginated pool is a result of slow transit of neutrophils against the mechanical forces of deformation.[27] In fact, the number of neutrophils found in the lung microcirculation is 40–65 times greater than that present in systemic blood vessels.[28] Since neutrophils have diameters of 6–8 μm, while the pulmonary capillaries are on the order of 2–15 μm, neutrophils often have to deform to transit through the pulmonary capillaries.[27,28] Compared with RBCs, neutrophils are larger and less deformable,[27] and when observed in vivo within the lung microcirculation, neutrophils are often elongated and ellipsoid in shape (**Fig. 4**).

We used Imaris (Bitplane; Zurich, Switzerland) to track and quantitatively analyze neutrophil transit within the pulmonary microcirculation using sequences of frames captured over a 5–10 min interval. Around 45 neutrophils were observed to transit through one field of view (260 μm x 260 μm) over a 5 min period (**Movie S2**). Tracks of individual neutrophils are shown in **Figure 4D** and are also included in **Movie S3**. These tracks were used to estimate the mean track speed and track length for each neutrophil and were plotted as a cumulative probability (**Fig. 4D**). Greater than 90% of neutrophils transited at 0.5 μm/s or less, indicating that a majority of neutrophils were slowly transiting through the capillaries (the mean speed was 0.26 μm/s). The mean track length for a neutrophil was 36 μm, or about 3 cell lengths (elongated neutrophils tended to be about 12 μm in length). About 90% of the neutrophils traveled 70 μm or less and the largest distance traveled was ~140 μm.

Discoid RBCs rapidly transit through the pulmonary microcirculation in live WT mice

We have visualized RBC trafficking through the pulmonary microcirculation using a fluorescent mAb Ter-119, which identifies a small glycophorin-A associated molecule specific to erythrocytes.[33] As shown in **Figure 5**, the transit of discoid RBCs in a feeding pulmonary arteriole is rapid and the RBCs appear as streaks in the upper portion of the vessel at t = 0 s. The subsequent frames demonstrate how a bolus of RBCs travels down the feeding arteriole to the arteriolar junction, and then disperses into the surrounding capillaries. The discoid shape of RBCs becomes more evident at the arteriolar junction, where RBCs slow down in order to deform and enter into the neighboring capillaries. Once inside capillaries, real-time movies demonstrate rapid transit of RBCs through the capillary bed at the time scale of a few seconds, 60x faster than slowly transiting neutrophils (see **Movie S4**) as shown previously.[29]

Post-acquisition spectral unmixing improves contrast of tricolor TPE images

We first established feasibility of imaging neutrophils, RBCs, and blood vessels simultaneously in the lungs of C57BL/6 WT mice (**Fig. 6A**). Visualizing three channels on a multiphoton system is not trivial, as one laser excitation wavelength is used to excite all three fluorochromes. To acquire dual color images (**Figs. 4 and 5**), we used excitation wavelengths of 920 nm and 940 nm to reduce tissue autofluorescence. The autofluorescence was strongest at lower excitation wavelengths (800–900 nm) and was indistinguishable from the fluorescence emitted by major green fluorochromes (FITC, GFP and Alexa Fluor 488). Simultaneous acquisition of three fluorochromes (FITC, Alexa Fluor 546 and Evans blue; **Fig. 6A**) necessitated decreasing our excitation wavelength to 850 nm to achieve an optimum TPE for all of the three fluorochromes. However, this strategy led to enhanced tissue autofluorescence, which contaminated the fluorescence emitted by FITC (**Fig. 6A**). Evans blue has been widely used as an intravascular dye for estimation of the vascular permeability induced during lung injury.[34] Evans blue, which has been used as an intravascular fluorochrome to visualize the cerebral microcirculation in vivo,[35] undergoes TPE at 850 nm and has a fluorescence emission spectrum that resembles Cy5 or Alexa Fluor 647 (far red channel). Although the fluorescence emission

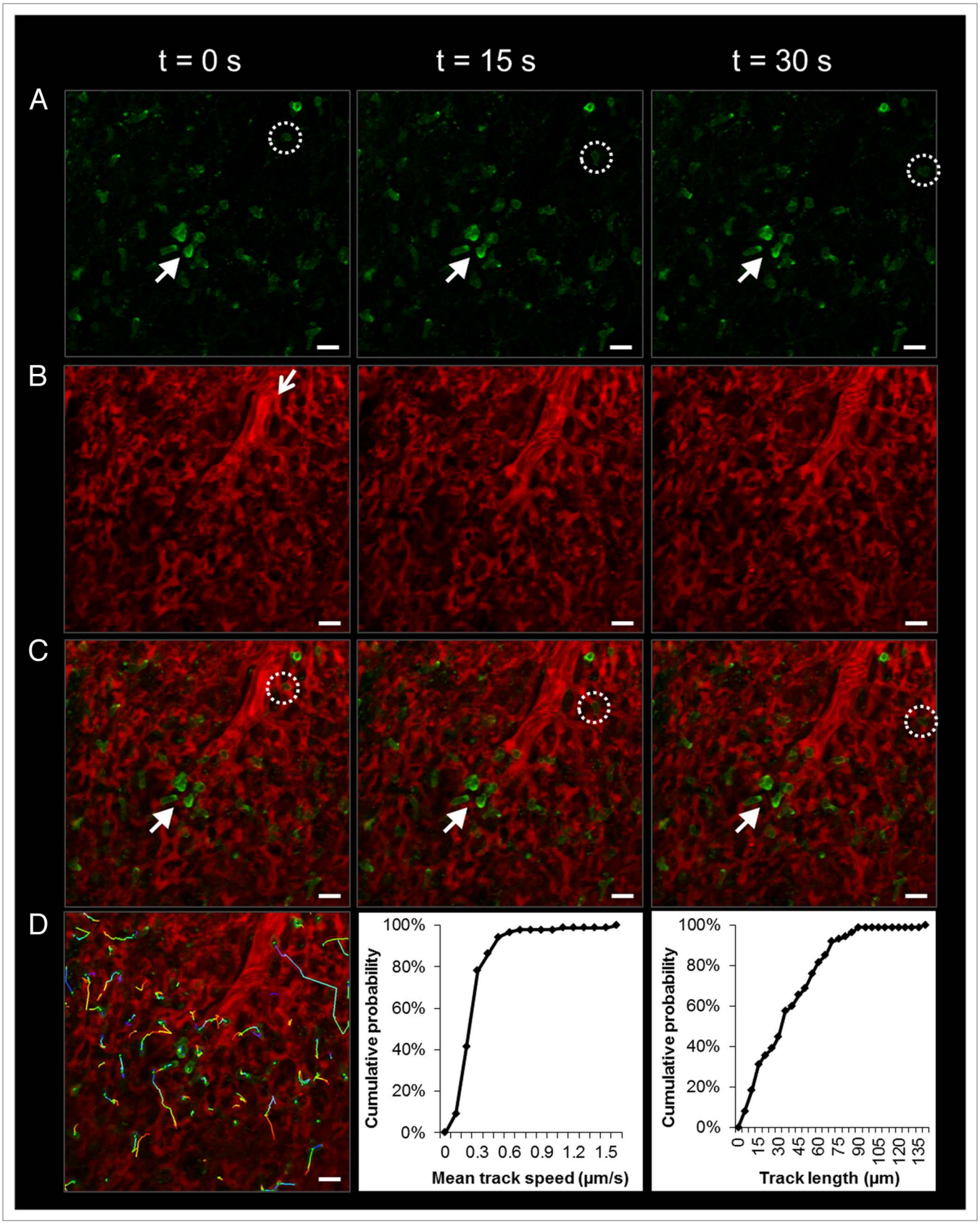

Figure 4 (see next page).

Figure 4. Elongated neutrophils slowly transit or rapidly 'hop' through the pulmonary capillaries of a live C57BL/6 mouse. (**A**) Green channel. Neutrophils (green) were stained by intravascular (iv) injection of FITC Ly-6G mAb. Solid arrow denotes slowly transiting neutrophils. The dotted circle highlights a neutrophil that travels much more rapidly and can be seen hopping between video frames. (**B**) Red channel. Texas Red-conjugated dextran (red) was administered iv to visualize pulmonary capillaries and a feeding arteriole. The open arrow shows the direction of blood flow within the feeding arteriole. (**C**) Merged dual color image. Neutrophils (green) are shown trafficking through pulmonary capillaries (red). Neutrophils take on an elongated shape that fills the lumen of pulmonary capillaries. (**D**) Individual tracks of transiting neutrophils tracked over a 5 min observation period using Imaris software are shown. The tracking video was analyzed in Imaris to extract mean track speed and track length for all the neutrophils and is plotted as cumulative distribution graphs. Note that greater than 90% of neutrophils migrate at 0.5 μm/s or less. The times displayed are relative to the selected video frames. Scale bars are 20 μm. The feeding arteriole has a diameter of 21 μm, while the capillaries have an average diameter of 6 ± 2 μm. The complete video sequences of neutrophil migration within pulmonary capillaries and the tracking video displaying neutrophils with attached dragon tails are included in **Movies S2 and S3**.

of Evans blue is strongest in the far red channel, it does bleed into the red channel to obscure the visualization of Alexa Fluor 546 Gr-1 stained neutrophils (**Fig. 6A**).

To enhance the visualization of RBC and neutrophil trafficking in tricolor images, we used a post-acquisition algorithm called spectral unmixing, which can be performed using commercial software such as NIS Elements. Spectral unmixing uses a least squares regression algorithm to appropriately segregate different spectral emission patterns associated with each fluorochrome and autofluorescence into their respective channels based on user defined reference spectra. **Figure 6B** demonstrates how spectral unmixing drastically improves the image quality by reducing autofluorescence in the FITC channel (green) and bleed through of the Evans blue (purple; far red channel) into the Alexa Fluor 546 (red) channel. The merged image (**Fig. 6B**) shows enhanced contrast of both RBCs and neutrophils. Unlike the unprocessed image (**Fig. 6A**), the image obtained post spectral unmixing (**Fig. 6B**) shows that neutrophils are visible as elongated red cells (positive for fluorescence) over dark background in the red channel and dark objects (absence of fluorescence) over a purple background in the far red channel.

RBC and neutrophil trafficking in the pulmonary microcirculation of live BERK non-sickle control and BERK SCD mice is similar in the absence of an inflammatory stimulus

We next performed simultaneous tricolor imaging to visualize RBC and neutrophil trafficking in live BERK non-sickle mice (a more appropriate control for our model) and BERK SCD mice. **Figure 7** shows rapid RBC trafficking visible as streaks throughout feeding arterioles. **Movies S5** and **S6** also show rapid RBC transit through pulmonary capillaries in both BERK control and SCD mice. Similar to **Figure 4**, neutrophil transit in both groups of mice was seen as a mixture of slowly transiting and fast hopping neutrophils. We did not observe any stasis in either BERK control or BERK SCD mice at baseline in the absence of a crisis. RBC and neutrophil trafficking in the pulmonary microcirculation was similar in BERK SCD and BERK non-sickle control mice in the absence of an inflammatory stimulus. These results also show that our experimental protocol enables intravital visualization of neutrophil and RBC trafficking in the pulmonary microcirculation of BERK sickle mice under physiological conditions with minimal surgical trauma. Any deviation from the homeostatic trafficking (**Fig. 7B**) following an inflammatory insult would be an effect of the inflammatory crisis induced by the stimulant.

Discussion

We have successfully visualized simultaneous neutrophil and RBC trafficking in the pulmonary microcirculation of live BERK non-sickle (control) and BERK SCD mice. We established that stasis is absent and cellular trafficking is similar in control and SCD mice in the absence of an inflammatory stimulus. These results are supported by previous studies[7,8,10] showing the absence of lung injury in SCD mice at steady-state. This study serves as the first step in establishing cellular trafficking at homeostasis in SCD mice and provides the experimental strategy that can be used to answer questions pertaining to the cellular and molecular mechanism of pulmonary vaso-occlusion in response to an inflammatory stimulus in future studies.

Maintenance of a physiological steady-state during intravital imaging is necessary for the successful interpretation of the results. Intravital imaging of SCD mice is challenging, as the thoracic surgery is invasive and the mice are anemic due to chronic hemolysis and organ infarction.[36] Although several studies have used intravital imaging to study the pulmonary microcirculation in rodents,[23,24,37-39] the experimental approach to enable visualization of immune cell trafficking in the intact lungs of live SCD mice has never been reported. Presson et al.[37] and Salaün et al.[38] provided methodologies to perform intravital imaging of the lung microcirculation in rats. Presson et al.[37] used a technique similar to that used in Looney et al.[23] and combined it with TPE to demonstrate increased leukocyte adhesion to the endothelium and vascular leakage in response to iv administration of 4b-phorbol 12-myristate 13-acetate (PMA) into rats. The advantage of using rats over mice is that rats are nearly ten times bigger than mice and more amenable to invasive surgery; however, a rat model of SCD does not exist. Salaün et al.[38] used fibered confocal fluorescence microscopy to investigate quantitative changes in pulmonary capillaries in response to induced emphysema in rats. Fluorescein-dextran was injected iv, a confocal probe was placed adjacent to the pleural surface and a vacuum was applied around the probe to keep the lungs inflated. The advantages of this technique are that it is minimally invasive and uses spontaneous breathing rather than mechanical ventilation. However, the lungs are freely moving and require stabilization by pressing onto the pleura, which can affect hemodynamics and lung perfusion. In the study by Yang et al.,[39] a combination of epifluorescence and brightfield microscopy was used to estimate the thickness of the glycocalyx within the pulmonary microcirculation of live

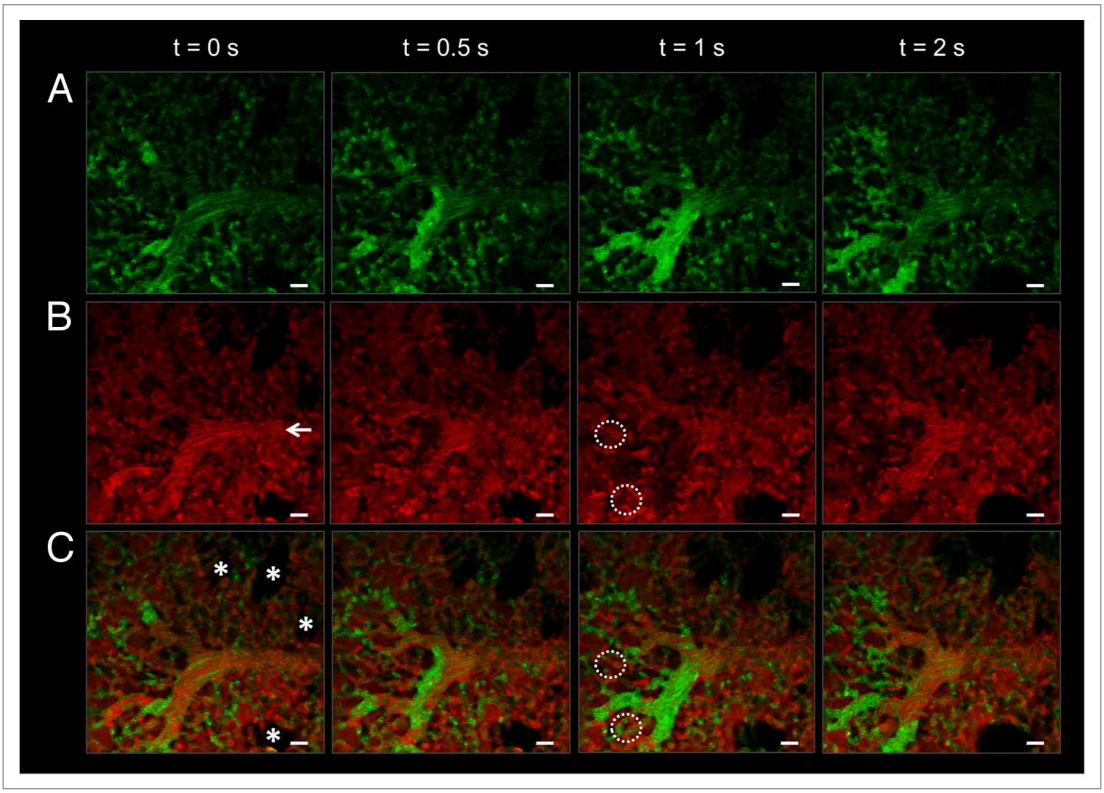

Figure 5. Discoid RBCs rapidly transit through the pulmonary microcirculation in a live C57BL/6 mouse. (**A**) Green channel. RBCs (green) were stained by iv administration of FITC Ter-119 mAb. (**B**) Red channel. Texas Red-conjugated dextran (red) was administered iv to visualize pulmonary capillaries and a feeding arteriole. The open arrow shows the direction of blood flow within the feeding arteriole. Note that Texas Red dextran fluorescence in the feeding arteriole decreases as a bolus of RBCs transits through it. (**C**) Merged dual color image. A t = 0 s, RBCs (green) can be seen traveling rapidly through the upper portion of the feeding arteriole (RBC transit is so rapid that their shape is distorted and they appear as green streaks in the image). Over the next 2 s, a bolus of RBCs (green) travels down the feeding arteriole and rapidly disperses into the capillaries. Since RBC transit is temporarily slowed at the arteriolar junction, the discoid shape of RBCs can be seen within the branches of the arterioles and within the capillaries. Dotted circles demonstrate that the presence of RBCs within capillaries is associated with dark spots or exclusion of the vascular dye within the capillaries. Alveoli are marked by asterisks. The times displayed are relative to the selected video frames. Scale bars are 20 μm. The feeding arteriole has a diameter of 29 μm, while the capillaries have an average diameter of 6 ± 2 μm. The complete video sequence of RBC trafficking within the pulmonary microcirculation is included in **Movie S4**.

mechanically ventilated mice. Applying a technique inspired by Kuebler et al.,[24] a cavity was made in the chest wall and the lung was brought into contact with a polymeric membrane containing a glass coverslip using a negative pressure. Free movement of the lung renders this preparation more physiological, but limits image capture to pauses between the breathing cycles, which affects temporal resolution. In addition, similar to Presson et al.,[37] this study also used two catheters and iv delivery of large amounts of supplemental fluids. These practices would not be ideal for SCD mice, which are anemic and cannot tolerate multiple cannulations. In addition, iv administration of fluids can substantially affect hematocrit, which can be detrimental for the survival of sickle mice.

In the current study, several key factors helped to maximize survival of SCD mice during the surgery. First, since the surgery is invasive, it is necessary to use injectable anesthetics followed by a maintenance anesthesia of 1% isoflurane with FiO_2 of 0.95. The most widely used injectable anesthetic cocktail of ketamine and xylazine alone can cause cardiac depression and a drop in arterial blood pressure, which can induce hypoxemia and/or hypercapnia in already anemic SCD mice. We used a cocktail of ketamine, xylazine and atropine, which has been recommended to achieve mean arterial blood pressures of greater than 50 mmHg during intravital microscopy of the mouse cremaster muscle.[40] Thus, it is necessary to monitor the arterial blood pressure of SCD mice during the intravital imaging (**Fig. 2**), so that all the observations are recorded under physiological conditions. Second, the bleeding during the thoracic surgery needs to be minimized by using a cauterizer to remove the overlying tissue and three to four anterior ribs in order to expose the left lobe of the lung. Use of scissors causes bleeding around the serrated ribs, leading to a drop in mean arterial blood pressure and hypovolemic shock. Third and finally, it is important that SCD mice receive adequate mechanical ventilation to optimally expand lungs and prevent hypoxemia. The P_{50} for the oxygen saturation of mouse hemoglobin is nearly 2-fold that of humans and use of FiO_2 higher than 0.21 is recommended to avoid hypoventilation of mice.[41] Since SCD mice are anemic, we have used FiO_2 of 0.95 for delivering maintenance anesthesia (1% isoflurane) to compensate for any uncertainty associated with optimal expansion of the lung during

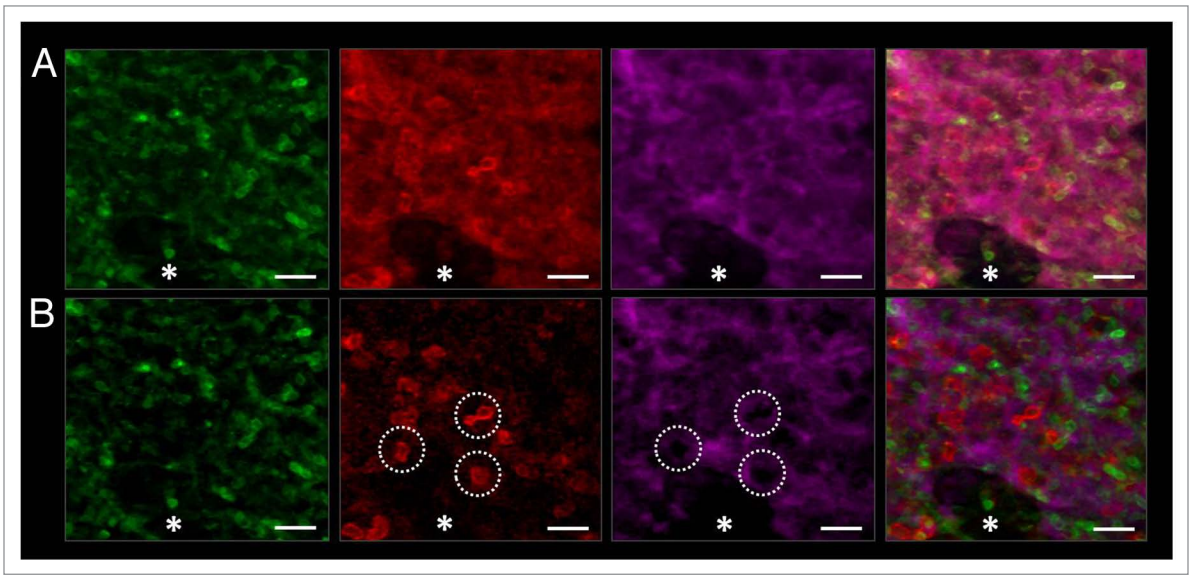

Figure 6. Post-acquisition spectral unmixing improves contrast of tricolor TPE images. Tricolor images of RBCs (green) and neutrophils (red) in the pulmonary microcirculation (purple) of a live C57BL/6 mouse (**A**) before spectral unmixing and (**B**) after spectral unmixing performed with NIS Elements software. The green channel shows RBCs stained with iv administration of FITC Ter-119 mAb. Spectral unmixing has served to reduce some tissue autofluorescence in the green channel, visible as a green haze in the original image A. The red channel shows neutrophils stained with iv administration of Alexa Fluor 546 Gr-1 mAb. The red channel also includes substantial bleed through from the intravascular fluorochrome (far red channel; purple) in the original image A. Spectral unmixing partially eliminates the bleed through, enabling visualization of neutrophils (red). After spectral unmixing, neutrophils appear as dark objects on a purple background far red (purple) channel. Three characteristic neutrophils are marked by the dotted circles. The merged tricolor images show that spectral unmixing leads to an improvement in visualization of both intravascular RBCs and neutrophils. Alveoli are marked by asterisks. Scale bars are 20 μm.

mechanical ventilation. It is recommended to use pulse oximetry[10] (**Fig. 2**), which allows noninvasive measurement of percent oxygen saturation of blood, in order to confirm the adequacy of ventilation.

There are several limitations associated with the current study. The Ter-119 mAb clone used to stain RBCs intravascularly identifies a small glycophorin-A-associated molecule on the surface of all erythrocytes from the proerythroblast to the mature erythrocyte stage.[33] Therefore, the Ter-119 mAb cannot differentiate between reticulocytes, dense sickling RBCs or irreversibly sickled cells (ISCs). It is important to note that RBCs in SCD are a heterogeneous population of at least four different types of cells,[4] which have different deformability depending on the concentration of HbS present in the cytoplasm. The difference in deformability of sRBC subtypes may play a role in their ability to adhere to neutrophils and the endothelium, and may impact their transit through pulmonary capillaries, which would be an interesting avenue of research provided these populations could be differentially labeled in vivo.

Although a resonant scanning head (like the one used in the current study) enables video rate acquisition of frames, improvement of the signal-to-noise ratio often requires averaging of line scans that reduces the frame acquisition rate. Without line averaging, our system is capable of acquiring 30 frames per second, but after introducing a 16x line average, we were limited to acquiring at 2 frames per second. This greatly affected our ability to accurately capture hopping neutrophil movement and fast transiting RBCs through arterioles and venules. Since hopping neutrophils can travel large distances between frames, automatic tracking software fails to track them and these cells require selection by hand in every frame. It is also not possible to track rapidly transiting RBCs in the larger vessels, since the tracking software requires identification of the user defined cell shape and the fast flowing RBCs are visible only as streaks (**Figs. 5 and 7**). To ameliorate this problem, we plan in future studies to reduce our field of view in the y direction (requiring fewer lines to be scanned per frame) for some acquisitions to enable higher frame rates (5 to 10 frames per second) for better cell tracking capabilities. As shown in a previous study,[23] the speed of blood flow within arterioles, venules, and also capillaries can be more directly assessed by injecting fluorescent micron-sized beads and performing a single rapid line scan acquisition perpendicular to the vessel of interest, which can be useful in confirming vaso-occlusion in our model.

Furthermore, our field of view is limited spatially and temporally. We only acquire in a single z plane because acquiring a z-stack increases acquisition time and decreases frame rate. Capillaries move in and out of the z plane with the breathing cycle, so we cannot continue tracking cells that enter a vessel perpendicular to the field of view. In addition, the lower half of the left lung is typically the region that is stabilized by the thoracic imaging window, since this area of the lung is the largest and also the farthest from the heart. However, imaging the lower half of the lung also seems like an advantage because it is known that intra-tracheal instillation of inflammatory stimulants and bacteria are primarily localized to lower lung zones.[42] The lower lung

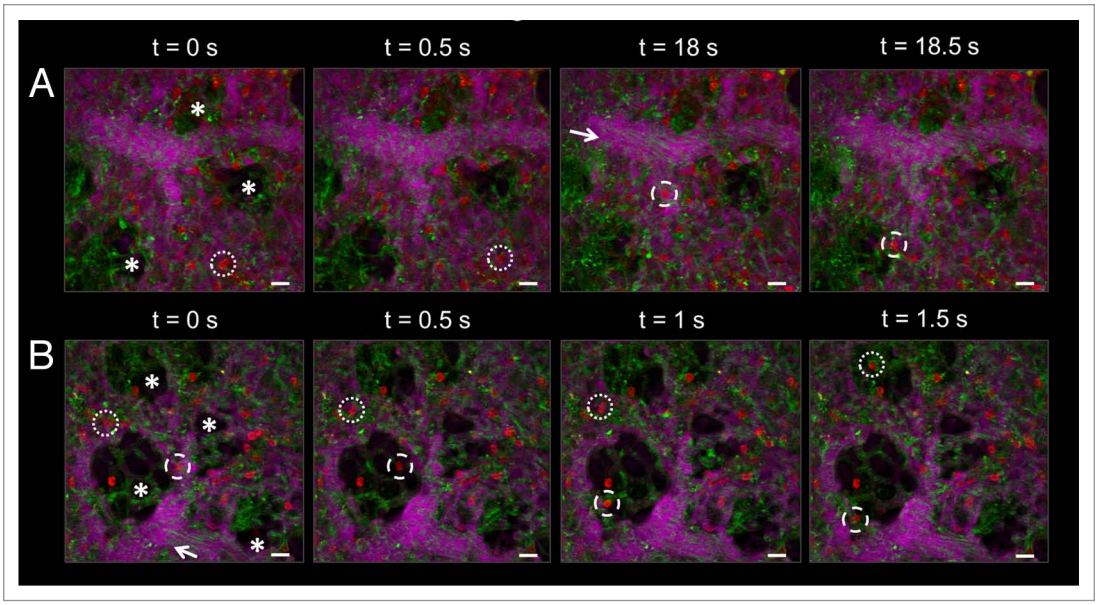

Figure 7. RBC and neutrophil trafficking in the pulmonary microcirculation of live BERK non-sickle control and BERK SCD mice is similar in the absence of an inflammatory stimulus. RBCs are shown in green, neutrophils in red, and the pulmonary microcirculation in purple. Alveoli are marked by asterisks and open arrows denote the direction of blood flow through feeding arterioles. (**A**) Cellular trafficking in the lungs of a live BERK non-sickle control mouse. Blood flow through the pulmonary arteriole is rapid, as seen by the green streaks of RBCs. Some neutrophils are seen slowly transiting, while others rapidly transit through capillaries and arterioles. Dotted circles highlight a hopping neutrophil rapidly transiting within a capillary from t = 0 s to t = 0.5 s. Dashed circles highlight another neutrophil that quickly exits the feeding arteriole and enters a capillary from t = 18 s to t = 18.5 s. The feeding arteriole has a diameter of 41 μm, while the capillaries have an average diameter of 5 ± 2 μm. (**B**) Cellular trafficking in the lungs of a live BERK SCD mouse. Perfusion in the SCD mouse is similar to the control non-sickle mouse shown in A. RBCs are visible as green streaks in the feeding arteriole. Dotted circles mark a hopping neutrophil as it transits quickly through capillaries over a period of 1.5 s. Dashed circles mark another hopping neutrophil as it exits the feeding arteriole and enters the capillaries surrounding an alveolus. Slowly transiting neutrophils were also observed in the pulmonary capillaries of the SCD mouse. The feeding arteriole has a diameter of 41 μm, while the capillaries have an average diameter of 7 ± 2 μm. The times displayed are relative to the selected video frames. Scale bars are 20 μm. The complete video sequence of RBC and neutrophil trafficking within the pulmonary microcirculation of a live BERK non-sickle control and live BERK SCD mouse are included **in Movies S5** and **S6.**

region also has more clinical relevance, since this area is typically where adult patients with ACS experience the most lung injury.[43] Furthermore, the thoracic surgery is very invasive, the mice cannot survive on the ventilator for several hours, and eventually the NIR laser can also cause tissue damage. Thus, it is possible to image a mouse lung for only 1 to 1.5 h.

In future studies, our setup will allow for visualizing vaso-occlusion in the lung in real-time following the addition of inflammatory stimuli such as lipopolysaccharide (LPS), live bacteria or intravascular hemin. Similar to the systemic vaso-occlusion seen in the cremaster muscle,[15] a recent study[8] has shown the presence of intravascular neutrophil-RBC congestion and neutrophil extracellular traps (NETs) formation in response to intravascular hemin administration in isolated fixed lung sections of SCD mice. It would be useful to repeat these studies in live mice with the intravital imaging approach proposed in the current study. This approach will enable elucidation of the molecular mechanism of pulmonary vaso-occlusion or congestion by analyzing the effect of function blocking mAbs and small molecule inhibitors against different adhesion molecules and receptors for DAMPs (danger associated molecular patterns) expressed on neutrophils, platelets, and endothelial cells. Several studies have shown that platelets may play a significant role in the thrombo-inflammatory process of vaso-occlusion in SCD.[16,44] Thus, it would be useful to simultaneously image platelets, neutrophils, RBCs and the vasculature, which can be achieved by proper selection of emission filters and a fluorochrome for the mAb against mouse CD49b, a recommended marker for in vivo platelet staining.[45]

The lack of an SCD mouse expressing a fluorescent protein like GFP in neutrophils, RBCs or platelets leaves us with the only option of using fluorescent Abs against markers for these cells. SCD mice are anemic and the intravascular administration of large volumes of reagents can alter the disease outcome by changing the hematocrit and extent of hemolysis. Thus, the total volume of reagents administered to the SCD mice should not exceed more than 20% of the total blood volume.[7] These concerns can be eliminated by crossing an SCD mouse with a reporter mouse expressing GFP in erythrocytes or *Lyz2-EGFP* mice[46] expressing GFP in neutrophils. However, BERK SCD and non-sickle control mice are on a mixed genetic background (H2b haplotype) with contributions from C57BL/6, 129Sv, FVB/N, DBA/2 and Black Swiss strains[19,36] and crossing these mice with other transgenic fluorescent reporter mice is nontrivial and tedious.

In conclusion, we report a TPE microscopy enabled intravital imaging approach that allows simultaneous visualization of leukocyte and RBC trafficking in the lungs of SCD mice. This approach will be helpful in future studies aimed at elucidating

the molecular and cellular mechanism of pulmonary vaso-occlusion in mouse models of SCD.

Materials and Methods

Reagents

Fluorescein-isothiocyanate (FITC) rat anti-mouse Ter-119 mAb (Clone Ter-119) and FITC rat anti-mouse Ly-6G mAb (Clone 1A8) were purchased from BD Biosciences (San Jose, CA). Rat anti-mouse Gr-1 mAb (clone RB6–8C5) was prepared from a hybridoma culture supernatant at the Lymphocyte Culture Center, University of Virginia. The Gr-1 mAb was conjugated to Alexa Fluor 546 using an antibody labeling kit from Molecular Probes, Inc. (Eugene, OR). Texas Red dextran (MW 70,000) and FITC dextran (MW 70,000) were also purchased from Molecular Probes Inc. Evans blue was purchased from Sigma Aldrich (Saint Louis, MO).

Mice

C57BL/6 WT mice, Berkeley (BERK) SCD mice (Tg[Hu-miniLCR$\alpha_1{}^G\gamma^A\gamma\delta\beta^S$], Hb$\alpha_m$−/− Hb$\beta_m$−/−) and BERK non-sickle control mice (Tg[Hu-miniLCR$\alpha_1{}^G\gamma^A\gamma\delta\beta^S$], Hb$\alpha_m$−/− Hb$\beta_m$+/−) were obtained from the Jackson Laboratory (Bar Harbor, ME) and housed in a specific pathogen-free animal facility at the University of Pittsburgh. BERK mouse phenotypes were confirmed in-house through assessment of complete blood counts (CBCs), percent reticulocytes, and hemoglobin electrophoresis. All animal experiments were approved by the Institutional Animal Care and Use Committee at the University of Pittsburgh.

Surgical preparation

Mice were anesthetized with an intraperitoneal (i.p.) injection of 125 mg kg^{-1} of body weight ketamine HCl (100 mg ml^{-1}; Henry Shein Animal Health; Dublin, OH), 12.5 mg kg^{-1} of body weight xylazine (20 mg ml^{-1}; LLOYD Laboratories; Shenandoah, IA), and 0.04 mg kg^{-1} of body weight atropine sulfate (0.54 mg ml^{-1}; Henry Schein Animal Health). When anesthetized, mice were given a 1 ml i.p. injection of warmed saline and placed on a heated stage in the supine position. A tracheotomy was performed and a short length of PE90 tubing was inserted into the incision site and tied to the trachea using a silk suture. Next, the right carotid artery was cannulated with heparinized PE10 tubing. Upon catheterization, mice were mechanically ventilated at 120 breaths min^{-1} with a tidal volume of 10 µl g^{-1} of body weight using a MiniVent Type 845 (Harvard Apparatus; Holliston, MA). The ventilator was used to deliver 1% maintenance isoflurane (Henry Shein Animal Health) with a FiO_2 of 0.95.

Mice were repositioned in the right lateral decubitus position. The left lobe of the lung was exposed through removal of the overlying skin, fat, and three to four anterior ribs. Bleeding was minimized by using a Thermal Cautery Unit (Geiger Medical Technologies; Council Bluffs, IA) during the lung surgery. Periodically during the surgery and imaging, the lung was rehydrated with physiological saline through the open cavity. To gently immobilize the lung, we used a micro-machined thoracic lung window inspired by Looney et al.[23] (**Fig. 2**), which provided a light suction through the use of a vacuum pump (Roscoe Medical Inc.; Strongsville, OH). The modified thoracic lung device had a larger viewing window (diameter ~5 mm) that allows more stable imaging over extended durations. A round coverslip (diameter 12 mm) was placed on top of the thoracic window and held in place using vacuum grease. Once the vacuum was applied, the thoracic window was gently lowered to immobilize a small region of the lower half of the left lung against the coverslip. Next, intravascular fluorescent dyes and fluorescent mAbs were injected through the carotid artery catheter. Intravascular fluorescent dyes included 200 µg of Texas Red dextran, 125 µg of FITC dextran or 75 µg of Evans blue. Neutrophils were labeled in vivo through injection of 7 µg of FITC-conjugated Ly-6G mAb or 7 µg of Alexa Fluor 546-conjugated Gr-1 mAb. A recent study has shown that lower amounts of fluorescent Ly-6G and Gr-1 (< 40 µg) facilitate real-time visualization of neutrophil recruitment in vivo without interfering with neutrophil recruitment.[47] RBCs were labeled in vivo with 35–40 µg of FITC-conjugated Ter-119 mAb, which identifies a small glycophorin-A associated molecule specific to erythrocytes.

TPE setup

Real-time two-photon movies of neutrophil and RBC trafficking within the lung microcirculation of live mice were captured using a Nikon A1R MP configured with the Nikon Ni-E upright motorized microscope (Nikon Instruments; Tokyo, Japan). The scope was equipped with a prechirped Chameleon Laser Vision (Coherent; Santa Clara, CA) capable of emitting excitation wavelengths from 700 to 1000 nm, an APO LWD 25x water immersion objective with 1.1 NA, a high speed resonant scan mode capable of acquiring at video rate (30 frames per second) without line averaging at 512 x 512 resolution, and a galvanometer scanning mode. A Nano-Drive (Mad City Labs Inc.; Madison, WI) allowed for fine high speed control of z-plane selection for image acquisition and a Prior automated stage controlled the x-y movement of the imaging platform. The fluorescence detection unit of the scope consisted of four detectors (photo multiplying tubes), which collected fluorescent light transmitted through 446 / 92 nm (detector 1; blue channel), 525 / 50 nm (detector 2; green channel), 576 / 26 nm (detector 3; red channel), and 685 / 70 nm (detector 4; far red channel) band pass filters, respectively. In this study, we used detector 2 for FITC, detector 3 for Texas Red or Alexa Fluor 546, and detector 4 for Evans blue. The microscope was also equipped with a metal halide (Intensilight) epifluorescent illuminator to view samples using the eyepieces. The microscope components including the laser, stage, resonant scanning head, detectors and acquisition were controlled using NIS-Elements software (Nikon Instruments; Tokyo, Japan) installed on a PC, which also allowed post-acquisition image processing of median filtering, averaging, cell tracking and spectral unmixing. The whole assembly of the TPE microscope was placed on a vibration isolation table (Kinetics Systems Inc., Boston, MA).

Intravital imaging

After administration of an intravascular fluorescent dye and fluorescent mAbs, mice were transported on the heated stage to the microscope stage. The microscope stage was enclosed in a temperature controlled black plexiglass enclosure set at 37 °C, which prevented interference by the ambient light. GenTeal eye

gel (Novartis; Basel, Switzerland; refractive index 1.33) was placed on the glass coverslip of the thoracic window device to interface with the two-photon objective. The eye gel has the same refractive index as water and is readily compatible with water immersion objectives. The approximate imaging plane was focused using the fluorescent lamp and eye piece, with fine adjustments made through the Nano-Drive and Prior stage following initiation of scanning in the resonant mode. Movies were acquired using NIS Elements software with the following settings: resonant scan mode with 16x line averaging (1.9 frames per second) and bi-directional scanning, laser power of 5%, and excitation wavelengths of 920 nm and 940 nm for dual color movies and 850 nm for tricolor movies. Acquisition was often conducted using a field of view of 512 μm x 512 μm or 260 μm x 260 μm at 1 or 0.5 μm resolutions, respectively.

Monitoring of physiological parameters

During image acquisition, several physiological parameters of mice were monitored (**Fig. 2**). To enable blood pressure measurements, the carotid artery catheter was connected to a blood pressure transducer (Edwards Lifesciences; Irvine, CA). The transducer was connected to the Power Lab / 8SP data acquisition system (ADInstruments; Colorado Springs, CO), the Quad Bridge amplifier (ADInstruments; Colorado Springs, CO), and finally to a computer monitor for real-time visualization and recording using LabChart software. The MouseOxPlus pulse oximeter and mouse thigh sensor (Starr Life Sciences Corp; Oakmont, PA) were used to measure oxygen saturation of blood, breath rate, breath distention, heart rate, and pulse distention.

Image processing

Movies were processed using Nikon's NIS Elements software. A median filter with a kernel size of 3 was applied over each video frame to improve signal-to-noise ratio. Signal contrast in each channel of a multicolor image was further enhanced by adjusting the maxima and minima of the intensity histogram of that channel. Spectral unmixing was performed using NIS Elements to separate out tissue autofluorescence from the FITC fluorescence and to reduce bleed through among different channels of tricolor images. To initiate spectral unmixing, region of interests (ROIs) were drawn over areas containing RBCs only (FITC), neutrophils only (Alexa Fluor 546), blood vessels only (Evans blue), and autofluorescence. The emission spectrum for each fluorochrome of interest was estimated within each ROI and saved. The saved spectra were used as reference spectra to unmix the contribution of each flurochrome to every pixel in the image using a least squares regression algorithm in NIS Elements.

Furthermore, neutrophil trafficking was analyzed using Imaris software (Bitplane; Zurich, Switzerland). Neutrophils were first isolated with the spots algorithm using shape criteria and a quality filter. False positive and false negative cells were manually adjusted in every frame. Tracks were created from the spot data over the 5 to 10 min movie and transit parameters such as mean track speed and track length were estimated. Quick time movies were also created in Imaris to show real-time tracking of neutrophils with dragon tails (**Movie S3**). Mean track speed and track length values from Imaris were imported into Microsoft Excel and cumulative probability graphs were created using the Data Analysis package.

Disclosure of Potential Conflict of Interests

There are no potential conflicts of interest to disclose.

Acknowledgments

This study was supported by 11SDG7340005 from the American Heart Association (P.S.), VMI startup funds (P.S.) and the NIH Pulmonary T32 training grant 2T32HL007563–26 (M.F.B).

Supplemental Materials

Supplemental materials may be found here:
www.landesbioscience.com/journals/intravital/article/29748

References

1. Brousseau DC, Panepinto JA, Nimmer M, Hoffmann RG. The number of people with sickle-cell disease in the United States: national and state estimates. Am J Hematol 2010; 85:77-8; PMID:20029951
2. Rees DC, Williams TN, Gladwin MT. Sickle-cell disease. Lancet 2010; 376:2018-31; PMID:21131035; http://dx.doi.org/10.1016/S0140-6736(10)61029-X
3. Barabino GA, Platt MO, Kaul DK. Sickle cell biomechanics. Annu Rev Biomed Eng 2010; 12:345-67; PMID:20455701; http://dx.doi.org/10.1146/annurev-bioeng-070909-105339
4. Kaul DK, Finnegan E, Barabino GA. Sickle red cell-endothelium interactions. Microcirculation 2009; 16:97-111; PMID:18720225; http://dx.doi.org/10.1080/10739680802279394
5. Belcher JD, Bryant CJ, Nguyen J, Bowlin PR, Kielbik MC, Bischof JC, Hebbel RP, Vercellotti GM. Transgenic sickle mice have vascular inflammation. Blood 2003; 101:3953-9; PMID:12543857; http://dx.doi.org/10.1182/blood-2002-10-3313
6. Holtzclaw JD, Jack D, Aguayo SM, Eckman JR, Roman J, Hsu LL. Enhanced pulmonary and systemic response to endotoxin in transgenic sickle mice. Am J Respir Crit Care Med 2004; 169:687-95; PMID:14684557; http://dx.doi.org/10.1164/rccm.200302-224OC
7. Belcher JD, Chen C, Nguyen J, Milbauer L, Abdulla F, Alayash AI, Smith A, Nath KA, Hebbel RP, Vercellotti GM. Heme triggers TLR4 signaling leading to endothelial cell activation and vaso-occlusion in murine sickle cell disease. Blood 2014; 123:377-90; PMID:24277079; http://dx.doi.org/10.1182/blood-2013-04-495887
8. Chen G, Zhang D, Fuchs TA, Manwani D, Wagner DD, Frenette PS. Heme-induced neutrophil extracellular traps contribute to the pathogenesis of sickle cell disease. Blood 2014; 123:3818-27; PMID:24620350; http://dx.doi.org/10.1182/blood-2013-10-529982
9. Gladwin MT, Sachdev V. Cardiovascular abnormalities in sickle cell disease. J Am Coll Cardiol 2012; 59:1123-33; PMID:22440212; http://dx.doi.org/10.1016/j.jacc.2011.10.900
10. Ghosh S, Adisa OA, Chappa P, Tan F, Jackson KA, Archer DR, Ofori-Acquah SF. Extracellular hemin crisis triggers acute chest syndrome in sickle mice. J Clin Invest 2013; 123:4809-20; PMID:24084741; http://dx.doi.org/10.1172/JCI64578
11. Ballas SK, Gupta K, Adams-Graves P. Sickle cell pain: a critical reappraisal. Blood 2012; 120:3647-56; PMID:22923496; http://dx.doi.org/10.1182/blood-2012-04-383430
12. Yale SH, Nagib N, Guthrie T. Approach to the vaso-occlusive crisis in adults with sickle cell disease. Am Fam Physician 2000; 61:1349-56, 1363-4; PMID:10735342
13. Desai PC, Ataga KI. The acute chest syndrome of sickle cell disease. Expert Opin Pharmacother 2013; 14:991-9; PMID:23534969; http://dx.doi.org/10.1517/14656566.2013.783570
14. Miller AC, Gladwin MT. Pulmonary complications of sickle cell disease. Am J Respir Crit Care Med 2012; 185:1154-65; PMID:22447965; http://dx.doi.org/10.1164/rccm.201111-2082CI
15. Hidalgo A, Chang J, Jang JE, Peired AJ, Chiang EY, Frenette PS. Heterotypic interactions enabled by polarized neutrophil microdomains mediate thromboinflammatory injury. Nat Med 2009; 15:384-91; PMID:19305412; http://dx.doi.org/10.1038/nm.1939
16. Li J, Kim K, Hahm E, Molokie R, Hay N, Gordeuk VR, Du X, Cho J. Neutrophil AKT2 regulates heterotypic cell-cell interactions during vascular inflammation. J Clin Invest 2014; 124:1483-96; PMID:24642468; http://dx.doi.org/10.1172/JCI72305
17. Embury SH, Matsui NM, Ramanujam S, Mayadas TN, Noguchi CT, Diwan BA, Mohandas N, Cheung AT. The contribution of endothelial cell P-selectin to the microvascular flow of mouse sickle erythrocytes in vivo. Blood 2004; 104:3378-85; PMID:15271798; http://dx.doi.org/10.1182/blood-2004-02-0713

18. Gutsaeva DR, Montero-Huerta P, Parkerson JB, Yerigenahally SD, Ikuta T, Head CA. Molecular mechanisms underlying synergistic adhesion of sickle red blood cells by hypoxia and low nitric oxide bioavailability. Blood 2014; 123:1917-26; PMID:24429338; http://dx.doi.org/10.1182/blood-2013-06-510180
19. Turhan A, Weiss LA, Mohandas N, Coller BS, Frenette PS. Primary role for adherent leukocytes in sickle cell vascular occlusion: a new paradigm. Proc Natl Acad Sci U S A 2002; 99:3047-51; PMID:11880644; http://dx.doi.org/10.1073/pnas.052522799
20. Manwani D, Frenette PS. Vaso-occlusion in sickle cell disease: pathophysiology and novel targeted therapies. Blood 2013; 122:3892-8; PMID:24052549; http://dx.doi.org/10.1182/blood-2013-05-498311
21. Ballas SK, Lieff S, Benjamin LJ, Dampier CD, Heeney MM, Hoppe C, Johnson CS, Rogers ZR, Smith-Whitley K, Wang WC, et al.; Investigators, Comprehensive Sickle Cell Centers. Definitions of the phenotypic manifestations of sickle cell disease. Am J Hematol 2010; 85:6-13; PMID:19902523
22. Looney MR, Bhattacharya J. Live imaging of the lung. Annu Rev Physiol 2014; 76:431-45; PMID:24245941; http://dx.doi.org/10.1146/annurev-physiol-021113-170331
23. Looney MR, Thornton EE, Sen D, Lamm WJ, Glenny RW, Krummel MF. Stabilized imaging of immune surveillance in the mouse lung. Nat Methods 2011; 8:91-6; PMID:21151136; http://dx.doi.org/10.1038/nmeth.1543
24. Tabuchi A, Mertens M, Kuppe H, Pries AR, Kuebler WM. Intravital microscopy of the murine pulmonary microcirculation. J Appl Physiol (1985) 2008; 104:338-46; PMID:18006870; http://dx.doi.org/10.1152/japplphysiol.00348.2007
25. Cella F, Diaspro A. Two-Photon Excitation Microscopy: A Superb Wizard for Fluorescence Imaging. In: Diaspro A, ed. Nanoscopy and Multidimensional Optical Fluorescence Microscopy. Boca Raton, FL: CRC Press, 2010:7-1-12.
26. Yipp BG, Petri B, Salina D, Jenne CN, Scott BN, Zbytnuik LD, Pittman K, Asaduzzaman M, Wu K, Meijndert HC, et al. Infection-induced NETosis is a dynamic process involving neutrophil multitasking in vivo. Nat Med 2012; 18:1386-93; PMID:22922410; http://dx.doi.org/10.1038/nm.2847
27. Doerschuk CM, Beyers N, Coxson HO, Wiggs B, Hogg JC. Comparison of neutrophil and capillary diameters and their relation to neutrophil sequestration in the lung. J Appl Physiol (1985) 1993; 74:3040-5; PMID:8366005
28. Doerschuk CM. Mechanisms of leukocyte sequestration in inflamed lungs. Microcirculation 2001; 8:71-88; PMID:11379793; http://dx.doi.org/10.1038/sj.mn.7300151
29. Huang Y, Doerschuk CM, Kamm RD. Computational modeling of RBC and neutrophil transit through the pulmonary capillaries. J Appl Physiol (1985) 2001; 90:545-64; PMID:11160053
30. Gebb SA, Graham JA, Hanger CC, Godbey PS, Capen RL, Doerschuk CM, Wagner WW Jr. Sites of leukocyte sequestration in the pulmonary microcirculation. J Appl Physiol (1985) 1995; 79:493-7; PMID:7592208
31. Kuebler WM, Kuhnle GE, Groh J, Goetz AE. Leukocyte kinetics in pulmonary microcirculation: intravital fluorescence microscopic study. J Appl Physiol (1985) 1994; 76:65-71; PMID:8175549
32. Lien DC, Henson PM, Capen RL, Henson JE, Hanson WL, Wagner WW Jr., Worthen GS. Neutrophil kinetics in the pulmonary microcirculation during acute inflammation. Lab Invest 1991; 65:145-59; PMID:1908922
33. Kina T, Ikuta K, Takayama E, Wada K, Majumdar AS, Weissman IL, Katsura Y. The monoclonal antibody TER-119 recognizes a molecule associated with glycophorin A and specifically marks the late stages of murine erythroid lineage. Br J Haematol 2000; 109:280-7; PMID:10848813; http://dx.doi.org/10.1046/j.1365-2141.2000.02037.x
34. Mammoto A, Mammoto T, Kanapathipillai M, Wing Yung C, Jiang E, Jiang A, Lofgren K, Gee EP, Ingber DE. Control of lung vascular permeability and endotoxin-induced pulmonary oedema by changes in extracellular matrix mechanics. Nat Commun 2013; 4:1759; PMID:23612300; http://dx.doi.org/10.1038/ncomms2774
35. Nacer A, Movila A, Baer K, Mikolajczak SA, Kappe SH, Frevert U. Neuroimmunological blood brain barrier opening in experimental cerebral malaria. PLoS Pathog 2012; 8:e1002982; PMID:23133375; http://dx.doi.org/10.1371/journal.ppat.1002982
36. Pászty C, Brion CM, Manci E, Witkowska HE, Stevens ME, Mohandas N, Rubin EM. Transgenic knockout mice with exclusively human sickle hemoglobin and sickle cell disease. Science 1997; 278:876-8; PMID:9346488; http://dx.doi.org/10.1126/science.278.5339.876
37. Presson RG Jr., Brown MB, Fisher AJ, Sandoval RM, Dunn KW, Lorenz KS, Delp EJ, Salama P, Molitoris BA, Petrache I. Two-photon imaging within the murine thorax without respiratory and cardiac motion artifact. Am J Pathol 2011; 179:75-82; PMID:21703395; http://dx.doi.org/10.1016/j.ajpath.2011.03.048
38. Salaün M, Modzelewski R, Marie J-P, Moreno-Swirc S, Bourg-Heckly G, Thiberville L. In vivo assessment of the pulmonary microcirculation in elastase-induced emphysema using probe-based confocal fluorescence microscopy. IntraVital 2012; 1:122-31; http://dx.doi.org/10.4161/intv.23471
39. Yang Y, Yang G, Schmidt EP. In vivo measurement of the mouse pulmonary endothelial surface layer. J Vis Exp 2013;72:e50322; PMID:23462690
40. Ley K, Mestas J, Pospieszalska M, Sundd P, Groisman A, Zarbock A. Intravital Microscopic Investigation of Leukocyte Interactions with the Blood Vessel Wall. Methods in Enzymology: Elsevier Academic Press, 2009:1-26.
41. Schwarte LA, Zuurbier CJ, Ince C. Mechanical ventilation of mice. Basic Res Cardiol 2000; 95:510-20; PMID:11192374; http://dx.doi.org/10.1007/s003950070029
42. Mizgerd JP, Skerrett SJ. Animal models of human pneumonia. Am J Physiol Lung Cell Mol Physiol 2008; 294:L387-98; PMID:18162603; http://dx.doi.org/10.1152/ajplung.00330.2007
43. Vichinsky EP, Styles LA, Colangelo LH, Wright EC, Castro O, Nickerson B; Cooperative Study of Sickle Cell Disease. Acute chest syndrome in sickle cell disease: clinical presentation and course. Blood 1997; 89:1787-92; PMID:9057664
44. Helms CC, Marvel M, Zhao W, Stahle M, Vest R, Kato GJ, Lee JS, Christ G, Gladwin MT, Hantgan RR, et al. Mechanisms of hemolysis-associated platelet activation. J Thromb Haemost 2013; 11:2148-54; PMID:24119131; http://dx.doi.org/10.1111/jth.12422
45. Jenne CN, Wong CH, Petri B, Kubes P. The use of spinning-disk confocal microscopy for the intravital analysis of platelet dynamics in response to systemic and local inflammation. PLoS One 2011; 6:e25109; PMID:21949865; http://dx.doi.org/10.1371/journal.pone.0025109
46. Faust N, Varas F, Kelly LM, Heck S, Graf T. Insertion of enhanced green fluorescent protein into the lysozyme gene creates mice with green fluorescent granulocytes and macrophages. Blood 2000; 96:719-26; PMID:10887140
47. Yipp BG, Kubes P. Antibodies against neutrophil LY6G do not inhibit leukocyte recruitment in mice in vivo. Blood 2013; 121:241-2; PMID:23287627; http://dx.doi.org/10.1182/blood-2012-09-454348